

Synthesis, Properties and Application of Polyimide by Rigid Semi-Alicyclic Structure

Yao Wang (王瑶), Rongwen Wang (王荣文), Guoli Tu* (屠国力)

Wuhan National Laboratory for Optoelectronics, Huazhong University of Science and Technology, 1037 Luoyu Road,
Wuhan430074, China

(湖北省武汉市珞喻路 1037 号华中科技大学武汉光电国家研究中心)

*Email: tgl@hust.edu.cn

Abstract

With the application of PI in flexible optoelectrical devices, many kinds of modified PIs are developed. A rigid semi-alicyclic functionalized isomeric diamine 5(6)-amino-1-(4-aminophenyl)-1,3,3-trimethylindane (5(6)-DAPI) was synthesized and separated by column to obtain 5-amino-1-(4-aminophenyl)-1,3,3-trimethylindane (5-DAPI), 6-amino-1-(4-aminophenyl)-1,3,3-trimethylindane (6-DAPI). A series of isomeric polyimides (CPI-x and TPI-x) were prepared by chemical imidation and thermal imidization. The effects of incorporation of isomeric rigid alicyclic structure into polymer backbones have been systematically investigated in terms of optical, thermal and mechanical properties, respectively. The bigger steric hindrance of 6-DAPI possessed stronger molecular interactions, and 6-DAPI series PIs exhibited better thermal stability. Meanwhile, due to the mild polymerization conditions of chemical imidization, the glass transition temperature (T_g) of the CPI-x series is in the range of 329-429 °C, which was higher than the T_g of TPI-x (321.9-370.7 °C).

Considering PIs based on 6FDA and HPMDA exhibited excellent optical properties and big CTE value. A rigid semi-alicyclic modified and fluorine-containing dianhydride: 9,10-difluoro-9,10-bis(trifluoromethyl)-9,10-dihydroanthracene-2,3,6,7-tetracarboxylic acid dianhydride (8FDA) was designed and synthesized. A series of PIs were prepared by the polymerization of 8FDA, 6FDA and HPMDA with two fluorine-containing diamines 2,2'-bis(trifluoromethyl)-4,4'-diaminobiphenyl (TFDB) and 4,4'-oxybis(3-(trifluoromethyl)aniline) (TFODA). The comparative research found that 8FDA-based PIs possessed higher glass transition temperature, thermal decomposition temperature ($T_g > 365$ °C) and better dimensional stability (coefficient of thermal expansion lower than 20 ppm K⁻¹) than the contrast PIs.

Colorless polyimide (cPI) films could be used to fabricate polymeric scattering substrate for flexible organic light-emitting diodes (OLEDs), which require no costly patterning, etching, or molding processes, aspects that are desirable for the commercialization of large-scale lighting panels. Systematic study of the influences of relative index of refraction, particle size, and doping concentration on transmittance and haze of transparent colorless polyimide(cPI) films was carried out. It was found that the reduction of transmittance and haze of the doped films decreases along with the decrease of the difference of refractive index between the particles and polymer matrix, and it could be compensated by the increase of particle size or doping.

Keywords: Rigid semi-alicyclic structure, Glass transition temperature, Coefficient of thermal expansion, nanoparticle, haze

1.1 Monomer synthesis of 5-DAPI, 6-DAPI.

The synthesis of DAPI is by acid-catalyzed dimerization of α -methylstyrene and subsequent nitration and reduction^[1], as shown in Fig 1.

1.2 Polymer preparation

A series of polyimide films were prepared by conventional thermal imidization and chemical imidization of 5-DAPI, 6-DAPI, isomeric 5(6)-DAPI with 6FDA, ODPA, BTDA, BPDA and PMDA,

respectively. For convenience, the PI films derived from thermal and chemical imidization are coded as CPI-x and TPI-x. The synthesis of the polymers was shown in Fig 2.

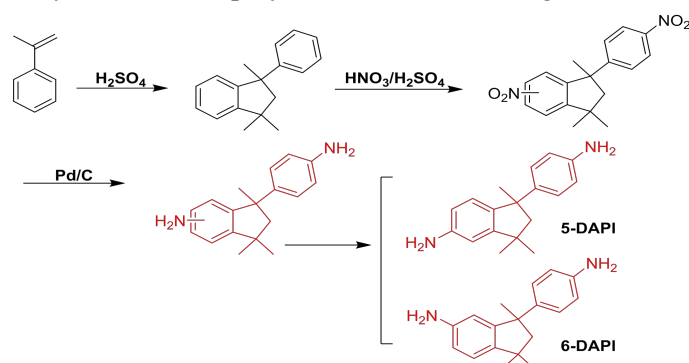


Fig 1. The synthesis process of 5-DAPI, 6-DAPI and 5(6)-DAPI

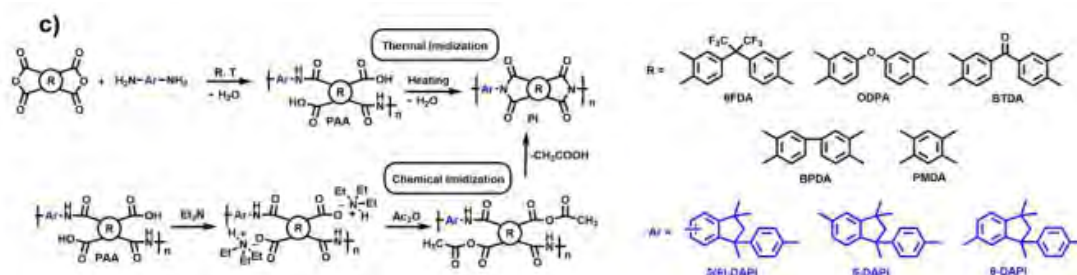


Fig 2. The synthesis of the polyimide films.

1.3 Results and discussion

1.3.1 Optical properties of PIs

The UV-Vis spectra of all CPI-x films and TPI-x films were shown in Fig 3 (a-b). The transmittance at 450 nm (T_{450}) and UV cutoff wavelength (λ_0) were summarized into Table 1. From the curve displayed in Fig. 3, by comparison, polyimides from 5-DAPI possessed best optical properties among 6-DAPI and 5(6)-DAPI PIs. The optical transparency differences between 5-DAPI, 6-DAPI and 5(6)-DAPI series are explainable by the decreased CTC formation. The presence of bigger dihedral angle of 5-DAPI can decrease the steric hindrance of backbone, break the conjugation of the polymer chain, increase the free volume and thus segments the charge transfer pathway^[2]. So that 5-DAPI series holding better transmittance than its analogous PIs. CPI-x enjoys higher optical transparency than its corresponding TPI-x. Due to the processing of thermal imidization, TPI-x was easy to occur crosslink between intermolecular chains, and increasing the packing degree, reducing the optical properties of TPI-x^[3]. Moreover, the CPI-x gets isotropic state of aggregation, and lower degree of crystallinity that contribute to its better transmittance.

1.3.2 Thermal properties of PIs

The thermal decomposition and stability of the TPI-x and CPI-x were evaluated by TGA and DMA. The results were shown in Table 1. From Table 1, we found that all 6-DAPI derived polymers had higher Tg values than corresponding 5-DAPI polymers, and the Tg of films originated from 5(6)-DAPI between the PIs behind. And the dates also indicated that the Tg of CPI-x was bigger than TPI-x. This might be attributed to steric hindrance of DAPI structure. PIs derive from the same dianhydrides based on 6-DAPI owned highest Tg values among these analogous PIs^[4]. Meanwhile Tg of CPI-x (CPI-4,ODPA/5-DAPI, 329.5°C) was bigger than homologous TPI-x (TPI-3,ODPA/5-DAPI, 321.9°C), which was attributed to different imidization processes. In the case of chemical imidization, water is not generated directly, and polymerization reacted at a moderate temperature and the presence of triethylamine makes the solution alkaline, meanwhile hydrolysis of the PAA is inhibited^[5]. Polymer with the same structure, the bigger molecular weight, the higher Tg, and CPI-x has bigger molecular weight lead to the Tg was significantly higher than the corresponding TPI-x. A typical set of TGA curves for CPI-(1-3) were depicted in Fig. 4 (d)-(f). No weight loss was detected until the temperature was scanned up to 480°C. The Td10 of CPI-x in N₂ stays in the range of

510-522°C. The results indicated that these PI films owned excellent thermal stability.

1.3.3 Mechanical and surface properties of the PIs

Mechanical properties of the PIs were summarized in Table 1. The depicted stress-strain curves were shown in Supporting Information Fig. 5. CPI-x series show tensile strengths at break of 45.7-103.0 MPa, elongation at break of 2.7-11.2%, and tensile modulus of 1.5-2.8 GPa. By contrast, TPI-x series showed tensile strengths of 16.0-80.7 MPa, elongation at break of 0.8-8.2%, and tensile modulus of 1.7-2.1 GPa. It was found that CPI-x displayed excellent mechanical properties than TPI-x. The larger tensile strengths, elongation at break and tensile modulus of CPI-x could be owed to their preparation process. PIs prepared from chemical imidization have a bigger molecular weight and longer chain, it's reported that PIs with the same structure, the longer molecular chain, the greater accumulation of the main chain it was. It was made the macromolecular hard to slide, and showing stronger rigidity, holding greater elastic modulus and tensile strengths [6]. Both series followed the tendency toward same dianhydride variation on the decreasing order for 5-DAPI > 5(6)-DAPI > 6-DAPI in terms of tensile strengths elongation at break, and tensile modulus.

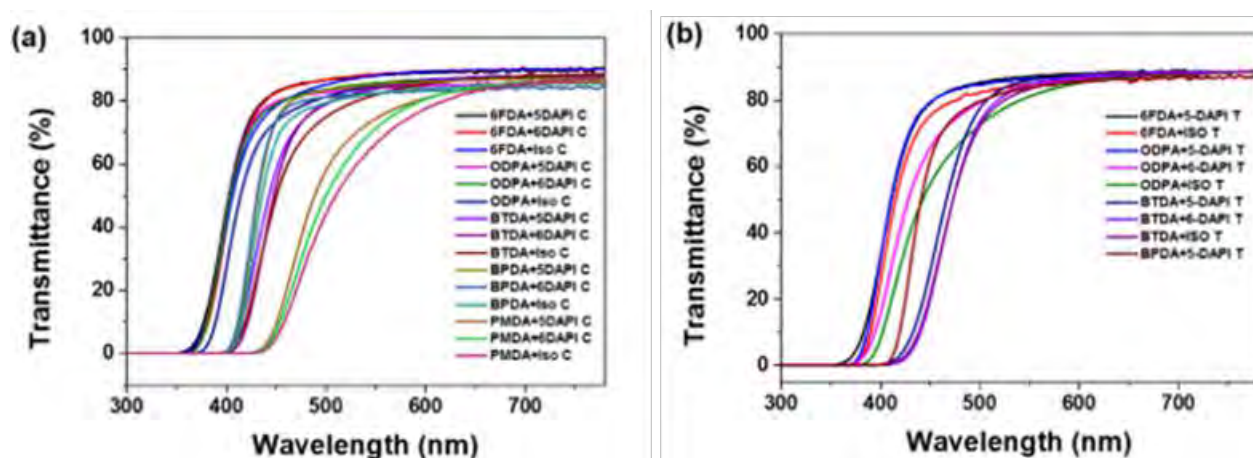


Fig 3. (a) The UV-Vis spectra of CPI films. (b) The UV-Vis spectra of TPI films.

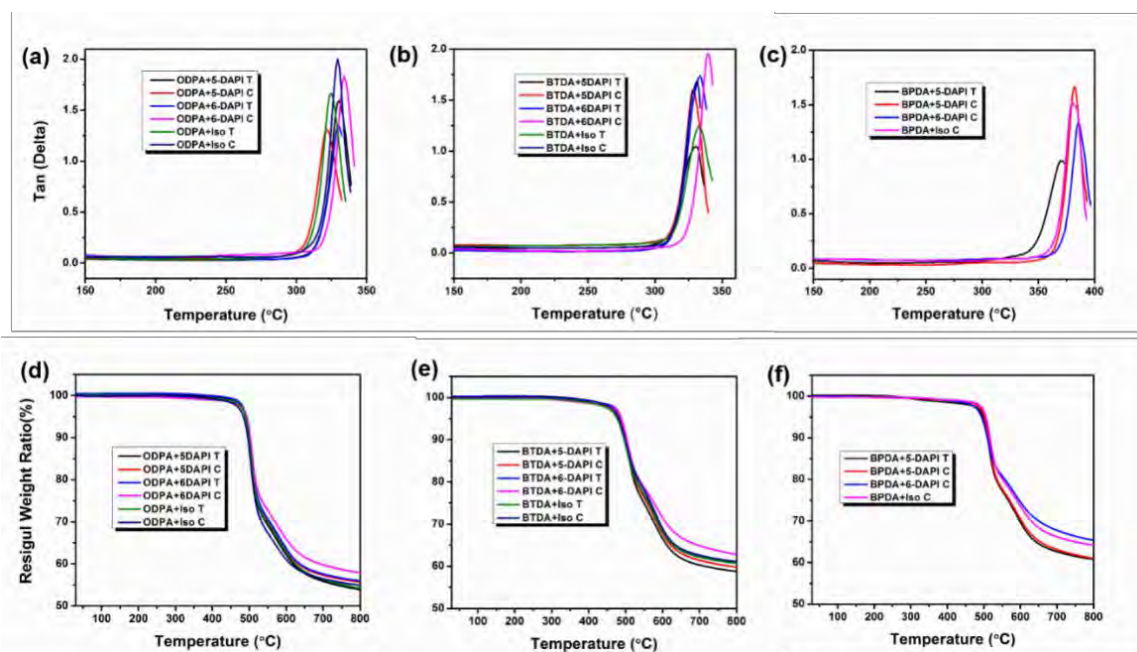


Fig 4. (a) DMA curves of the polyimides based on ODPA and DAPI. (b) DMA curves of the polyimides based on BTDA and DAPI. (c) DMA curves of the polyimides based on BPDA and DAPI. (d) TGA curves of the polyimides based on ODPA and DAPI. (e) TGA curves of the polyimides based on BTDA and DAPI. (f) TGA curves of the polyimides based on PMDA and DAPI

Table 1. The thermal, mechanical and optical properties of PIs.

Polymer	Dianhydride	Diamine	Thermal properties				Mechanical properties ^a			Optical Properties	
			T _g (°C)	T _{d5}	T _{d10}	Char	T _s	E _b	T _m	T ₄₅₀ ^c	λ ₀ ^d
TPI-1	6FDA	5DAPI	333.3	493	508	56.2	33.7	2.8	1.7	79.1	365
CPI-1	6FDA	5DAPI	333.1	494	510	57.9	91.6	8.8	2.1	82.9	361
CPI-2	6FDA	6DAPI	345.2	504	522	56.1	53.8	4.8	1.5	82.6	366
TPI-2	6FDA	Isomer	342.1	494	510	57.9	25.6	1.2	2.1	75.3	377
CPI-3	6FDA	Isomer	335.9	496	512	57.1	56.2	4.1	2.1	78.5	365
TPI-3	ODPA	5DAPI	321.9	484	496	54.2	74.8	7.6	2.1	79.4	374
CPI-4	ODPA	5DAPI	329.5	489	500	54.2	88.4	10.4	2.0	79.7	368
TPI-4	ODPA	6DAPI	329.7	491	500	55.7	69.6	4.6	2.2	75.3	378
CPI-5	ODPA	6DAPI	334.0	494	503	58.2	70.1	5.3	2.0	78.9	369
TPI-5	ODPA	Isomer	324.8	490	500	55.7	77.1	6.1	1.8	65.5	377
CPI-6	ODPA	Isomer	330.4	491	500	53.9	88.4	5.7	2.1	73.5	377
TPI-6	BTDA	5DAPI	330.7	479	497	61.1	80.7	10.6	1.9	28.0	410
CPI-7	BTDA	5DAPI	329.1	482	499	60.2	88.2	8.3	2.3	57.5	401
TPI-7	BTDA	6DAPI	339.0	487	502	60.7	23.6	1.1	2.1	19.6	419
CPI-8	BTDA	6DAPI	333.5	488	503	62.8	45.7	2.7	1.9	52.9	407
TPI-8	BTDA	Isomer	332.3	485	499	58.5	16.0	0.8	2.1	20.9	416
CPI-9	BTDA	Isomer	331.4	486	501	59.8	68.7	3.9	2.6	49.4	404
TPI-9	BPDA	5DAPI	370.7	493	510	58.5	70.0	5.7	2.0	61.5	408
CPI-10	BPDA	5DAPI	379.7	497	510	60.6	103.0	7.4	2.8	73.6	402
CPI-11	BPDA	6DAPI	385.5	505	516	64.2	68.6	4.3	2.3	73.4	401
CPI-12	BPDA	Isomer	382.7	501	513	61.0	68.7	3.9	2.6	67.0	404
CPI-13	PMDA	5DAPI	423.7	486	498	53.1	70.8	9.0	1.9	9.2	433
CPI-14	PMDA	6DAPI	429.1	491	504	56.9	69.0	5.5	2.0	6.8	435
CPI-15	PMDA	Isomer	422.9	490	502	55.6	71.0	7.5	1.9	4.7	438

^a T_s, tensile strength; E_b, elongation at break; T_m, tensile modulus.

^b Residual weight percentage at 800 °C in N₂.

^c Transmittance at 450 nm.

^d UV-vis cutoff wavelength.

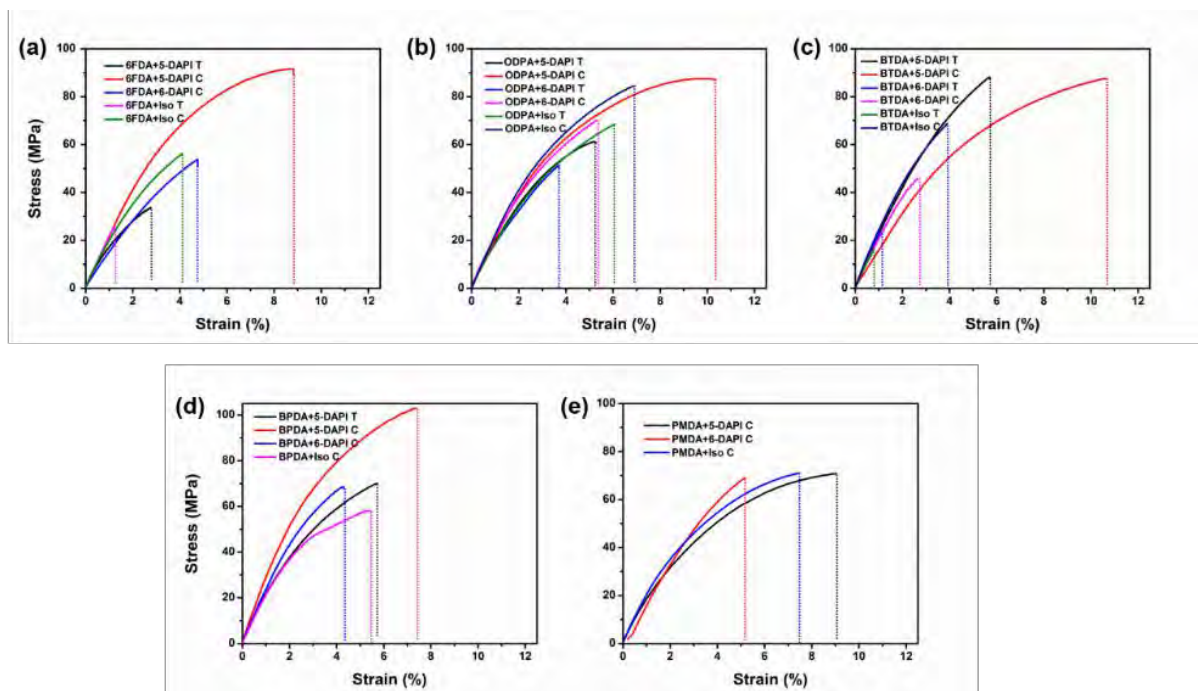


Fig 5. (a) Stress and strain curve of polyimide films based on 6FDA and DAPI. (b) Stress and strain curve of polyimide films based on ODA and DAPI. (c) Stress and strain curve of polyimide films based on BTDA and DAPI. (d) Stress and strain curve of polyimide films based on BPDA and DAPI. (e) Stress and strain curve of polyimide films based on PMDA and DAPI.

2.1 Monomer Synthesis of 8FDA

8FDA was prepared by five-step synthesis, as shown in Fig.6.

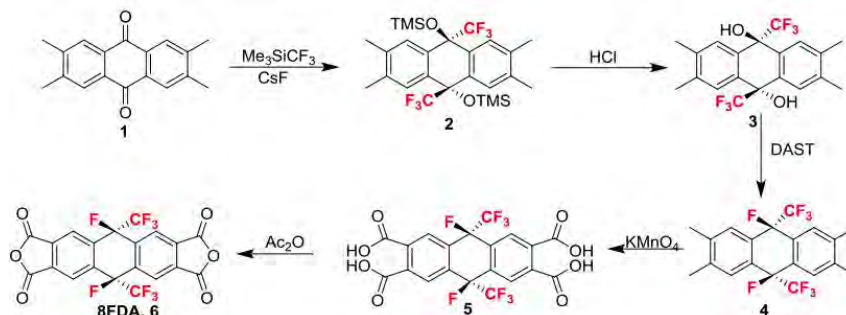


Fig 6. Synthetic route to 8FDA.

2.2 Polymer preparation

A series of polyimide films was prepared by conventional thermal imidization of 8FDA, 6FDA, and HPMDA with TFDB and TFODA, respectively. For convenience, the PI films derived from 8FDA, 6FDA, and HPMDA are coded as PI-x. The synthesis of the polyimides based on 8FDA, 6FDA, and HPMDA were shown in Fig 7.

2.3 Results and Discussion

2.3.1 Optical Properties of PIs

The UV-Visible spectra of all films were shown in Figure 8a, and the transmittance at 400 nm (T_{400}) and cutoff wavelength (λ_0) were summarized in Table 2, and, according to Fig 8a, 8FDA-based films exhibited T_{400} from 46% to 64% and λ_0 below 345 nm. onally, 6FDA series films showed T_{400} from

38% to 74% and λ_0 below 360 nm. Meanwhile, PIs that originated from HPMDA exhibited T_{400} from 79% to 83% and λ_0 below 295 nm. The T_{400} of PIs with the same diamines decreased in the order of HPMDA > 6FDA > 8FDA.

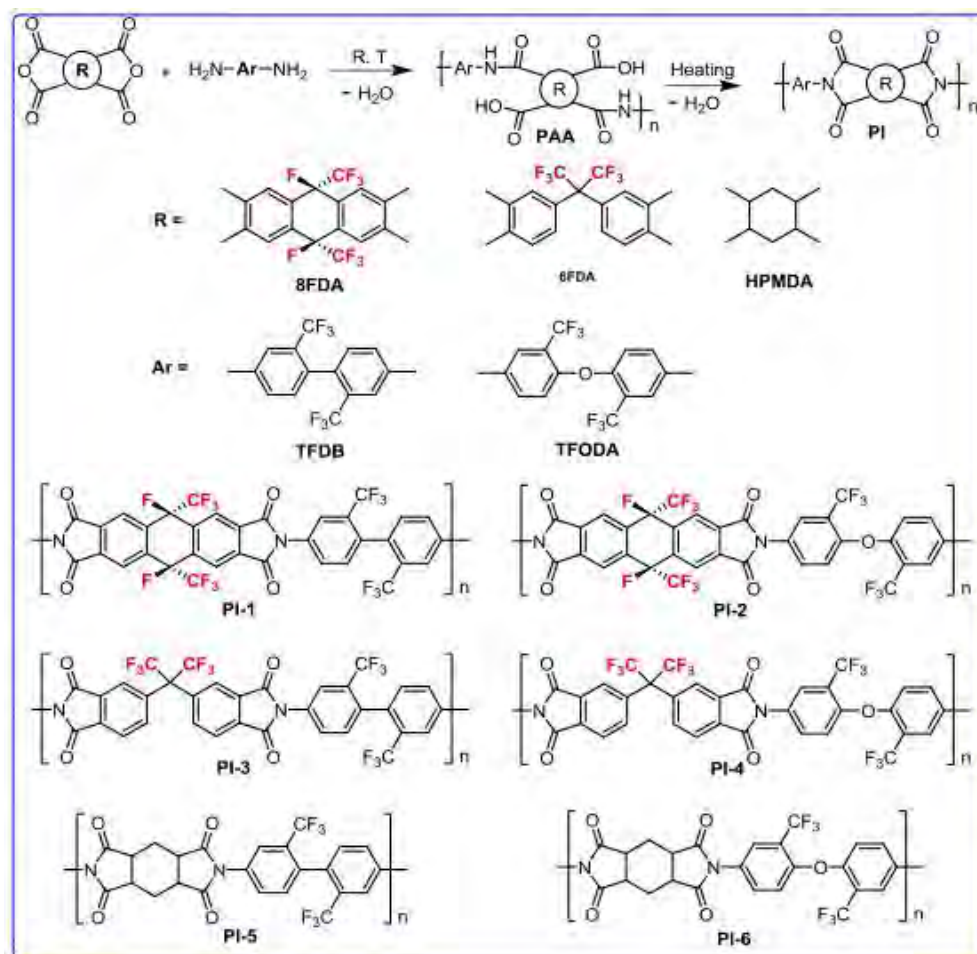


Fig 7. Synthesis of polyimides based on 8FDA, 6FDA, and HPMDA.

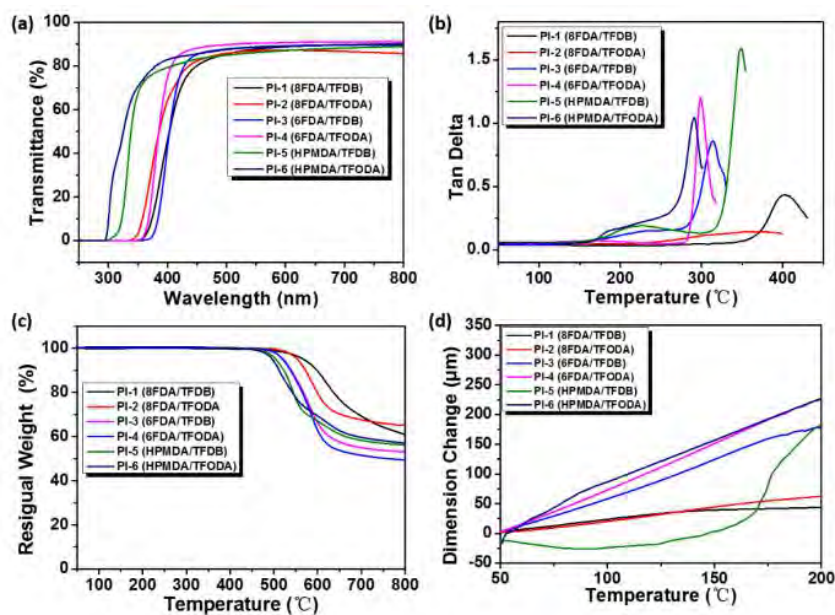


Fig 8. (a) The UV-Vis spectra of CPI films; (b) the DMA curves of PI films; (c) the TGA curves of PI films; and (d) the TMA curves of PI films.

2.3.2 Thermal Properties of PIs

The thermal decomposition and stability properties of the films of PIs were evaluated by thermogravimetric analysis (TGA), dynamic mechanical analysis (DMA), and thermal mechanical analysis (TMA). All data were obtained from the PIs films, and are shown in Table 2. According to the DMA curve in Figure 8b, it was found that 8FDA-based PIs exhibited higher Tg values than the corresponding 6FDA-based and HPMDA-based PIs films. The Tg values of PI-1 and PI-2 were in the range of 369–401 °C, while the Tg of the contrast PIs (PI-3 to PI-6) were in the range of 292–348 °C. The Tg of PI-1 is 401 °C, which is 86 °C higher than that of PI-3. This can be attributed to the rigid structure of 8FDA monomer. According to the single crystal structure, 8FDA has 1,4-cyclohexadiene as the bridge between two phenyl anhydrides. The planarity of 8FDA is much better than that of 6FDA and HPMDA, with a bridge of quaternary carbon between two phenyl anhydrides and alicyclic structure. The linear structure, rigidity, and inter-chain interaction of 8FDA-based PIs were stronger than the PIs based on 6FDA and HPMDA [7]. According to the literature, the Tg of polyimides were dictated by the chain rigidity, as well as the inter- and intra-molecular interactions that originated from the CTC between the electron-withdrawing dianhydride residue and the electron-donating diamine residue [8]. For a given dianhydride, the Tg value of PIs were in the order of TFDB > TFODA. Because the rigidity of TFODA, which consisted of flexible ether, the bond was lower than TFDB.

As shown in Table 2 and Fig 8c, no significant weight loss was detected until the temperature was as high as 460 °C. The 1% weight loss temperature (T_{d1}) and the char yield of these polyimides ranged from 462 to 518 °C and 50%–64%, respectively. 8FDA-based PIs exhibited higher T_{d1} more values than the corresponding 6FDA and HPMDA films.

The 5% weight loss temperature (T_{d5}) of PI-x in N2 stayed in the range of 497–557 °C. The curves in Fig.8c indicated that the thermal stability of PI-x originated from the same dianhydride decreased in the order of TFDB and TFODA. It can be accounted for that TFDB-based PIs possessed higher rigidity and showed good thermal stability.

The TMA results are shown in Table 3 and Figure8d. The CTE values of PI-1 and PI-2 derived from 8FDA were 14 to 18 ppm K⁻¹, respectively, while the contrast PIs based on 6FDA and HPMDA ranged from 44 to 63 ppm K⁻¹. Compared with 6FDA and HPMDA, it is the bent-shaped rigid dianhydride moiety containing cis-type 1,4-cyclohexadiene skeleton that suppress CTE. It has been reported that inhibition of the mobility of molecular segments is important for reducing the CTE^[9-10]. Compared with PIs based on 6FDA and HPMDA, PIs derived from 8FDA have a better linear structure, and stronger intermolecular interactions will inhibit molecular mobility and increase intrachain orientation, so 8FDA-based PIs have better dimensional stability.

2.3.3 Mechanical Properties

Mechanical properties of the PIs are summarized in Table 2. PI-1 and PI-2 showed the tensile strengths at break of 96.0–113.0 MPa, the elongation at break of 2.1–7.0%, and the tensile modulus of 1.2–4.5 GPa. As a comparison, PI-3 to PI-6 showed lower tensile strengths at break of 39.0–84.0 MPa, comparable elongation at break of 2.7–5.8%, and lower tensile modulus of 1.1–1.8 GPa. It can be explained that molecular structure of 8FDA, which was bridged by multi-substitute 1,4-cyclohexadiene segment, was more planar and regular than 6FDA and HPMDA. These characters made 8FDA-based PIs exhibit stronger rigidity and closer accumulation. The structure characters of 8FDA enhanced its mechanical properties.

Table 2. The thermal resistant, mechanical, optical, and surface properties of PI films.

Polym er	Dianhydride	Dianmin e	Thermal Properties				Mechanical Properties ^a				Optical Properties	
			T_g (°C) DMA	T_{d1} (°C)	T_{d5} (°C)	Char Yield (%) ^b	CTE (ppm K ⁻¹) ^c	T_s (MPa)	E_b (%)	T_m (GPa)	T_{400} ^d (%)	λ_0 ^e (nm)
PI-1	8FDA	TFDB	401	518	557	64	14.49	113	7.0	1.2	46	358
PI-2	8FDA	TFODA	369	492	550	60	18.31	96	2.1	4.5	64	344
PI-3	6FDA	TFDB	315	488	521	53	48.70	84	3.3	2.6	43	370
PI-4	6FDA	TFODA	300	490	520	50	62.53	65	5.8	1.1	71	353
PI-5	HPMDA	TFDB	292	473	501	56	44.12	71	4.0	1.8	79	304
PI-6	HPMDA	TFODA	348	462	497	57	63.59	39	2.7	1.8	83	296

a T_s , tensile strength; E_b , elongation at break; T_m , tensile modulus;

b residual weight percentage at 800 °C in N₂;

c coefficient of thermal expansion along the X-Y direction, measured in the range of 50-200 °C at a heating rate of 5 K min⁻¹;

d transmittance at 400 nm

e UV-vis cutoff wavelength.

3.1. Fabrication of cPI films with nanoparticles

3.1.1. Doping nanoparticles in cPI

The weight ratio of nanoparticles regarding to the weight of cPI were 0 wt%, 0.5 wt%, 1.0 wt%, and 3.0wt%. The ultrasonic dispersion method described below was used to obtain the uniform nanoparticle dispersion solutions. Nanoparticles (300 mg for cPI-1, 273 mg for cPI-2, Al₂O₃ 200 nm or SiO₂ 200-300 nm or SiO₂ 400-600 nm, Aladdin Industrial Co.) and half weight of the solvent (20 g, DMAc for cPI-1, NMP for cPI-2, HPLC grade, J&K Scientific, Ltd.) were added in a 100 mL two-necked flask, and then the mixture was sonicated (SB-5200D, 40 kHz, 300 W) at room temperature for 30 min to disperse nanoparticles. Then the two-neck flask was transferred to a mechanical stirrer (HeidolphRZR2102 control Z). cPI (10 g for cPI-1, 9.07 g for cPI-2) was added into the mixture which was being stirred. After that, the remaining half of the solvent (20 g, DMAc for cPI-1, NMP for cPI-2, HPLC grade, &K Scientific, Ltd.) was added. Then the solution was stirred overnight at room temperature. The viscosity of solutions were measured to be in the range from 10000 to 11000 cP (Brookfield DVII+ Pro) at room temperature. The solution was filtered with sandcore funnel (Beijing Synthware Glass, Inc., G2, porous size: 10-15µm), and allowed to stand for more than 2 h to get rid of air bubbles prior to use.

3.1.2. Thermal imidization to form cPI films

The wet films were prepared by spin coating at room temperature. Before coating, a proper amount of solution (about 1 mL) was dropped to the center of substrate (50×50 mm² float glass, ultrasonic cleaned with acetone, isopropanol, and deionized water, blown dry with dry nitrogen gas) that fixed on the spin coater (KW-4B, SETCAS Electronics Co., Ltd.). The spin coating process consists of two steps: the low-speed step (fixed at 500 rpm, 9s) to spread solution to the whole substrate, and the high-speed step (range from 1000 to 3000 rpm, 60 s) to get a film with uniform thickness. After that, the wet films were transferred to the preheated (80 °C) oven and placed horizontally. Subsequently,

step-heating procedures were performed, and 30 min of each stage includes both the heating time and the holding time. It usually takes about 9 min to raise the temperature by 30 °C.

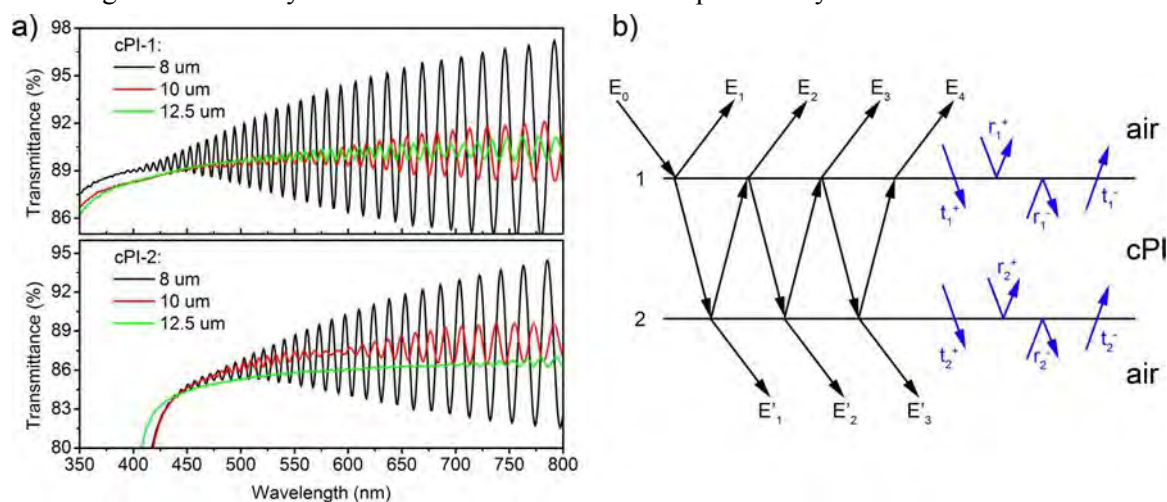


Figure 9. a) Transmittance of pure cPI films with different thickness (measured in normal direction). b) Schematic diagram of equal inclination interference.

For the films made from cPI-1, which is a resin and has finished chemical imidization during the synthesis, the only purpose of heat treatment is to remove the solvent (the boiling point of DMAc is about 166 °C). When it comes to the films made from cPI-2, in addition to removing the solvent (the boiling point of NMP is about 203 °C) during the heat treatment, it is also important to complete the thermal imidization. After annealing, the samples were freely cooled to room temperature. By cutting the edges of the samples and immersing them in deionized water (about three to 5 min), the cPI films were obtained.

3.2. Result and Discussion

3.2.1. Thickness

The thickness of the transparent colorless polyimide films for OLEDs is microscale, ranging from 5 to 25 μm. The transmittance is one of the key parameters when they are utilized in flexible OLEDs. In this work, PI films with thicknesses ranging from 5 to 20 μm by controlling the spin speed (high speed step) were actually prepared. But the film with thicknesses less than 8 μm needed a really long time to peel off the substrate by DI water, and they were too soft to be self-supporting. To prepare cPI films with thickness larger than 20 μm, we would have to increase the viscosity of the solutions by increasing solid content or use lower spin speed, but these were not practical. On the one hand, further increasing the viscosity of the solutions will make filtration more difficult. However, the use of a lower spin speed will result in a nonuniform film thickness. Several representative thicknesses of 8 (almost the thinnest to self-support), 10, and 12.5 μm (the most commonly used thickness for applications) were selected for analysis.

The transmittance mainly depends on the thickness of the film (d) and the refractive index of the cPI materials according to Figure 9b and eq 1^[11]. By comparing the transmittance of pure cPI films (doped at concentration of 0wt%) with different thickness in Figure 9a, it was found that the transmittance varies with the film thickness and the wavelength of the incident light. The transmittance spectra have shown larger oscillation periods and amplitudes with the increase of the incident light wavelength.

$$T = \frac{8n^2}{1 + 6n^2 + n^4 - (n^2 - 1)^2 \cos(4\pi nd/\lambda)} \quad (1)$$

The oscillation periods also increased with the decreasing thickness of the films. These phenomena can be explained by the theory of film interference and would somehow influence on device performance when cPI films are used in light emitting devices. When used as transparent substrate in flexible device, it would be better to use them with thickness not less than 12.5 μm specific to these two kinds of polyimide films.

3.2.2 Dispersion of Nanoparticles

It should be mentioned that it is unlikely that fully monodisperse nanoparticles could be readily obtained. Since agglomeration of nanoparticles is unavoidable without surface modification (new components will be brought in), we only need to ensure that most of the particles are well dispersed. Figure 10 exhibits the cross-sectional SEM images and optical microscopic images of cPI films doped with Al_2O_3 200 nm, SiO_2 200-300 nm, and SiO_2 400-600 nm with the concentration of 3.0wt%, respectively. The SEM images indicate that most of the particles are properly dispersed in the polymer matrix. It should be noted that the shapes of some particles were changed because of the thin Au capping layer deposited before SEM measurement. Furthermore, the absolute numbers of particles were small at such a doping concentration, which resulted in the small probability of finding multiple particles in the same visual field. The white dots in the optical microscopic images denoted the nanoparticles doped in cPI films. According to these images, we can also conclude that most of the nanoparticles were properly dispersed in the films, and the logarithmic FFT patterns further confirmed this. At the same time, the existence of some large white spots in the optical microscopic images should not be simply ignored.

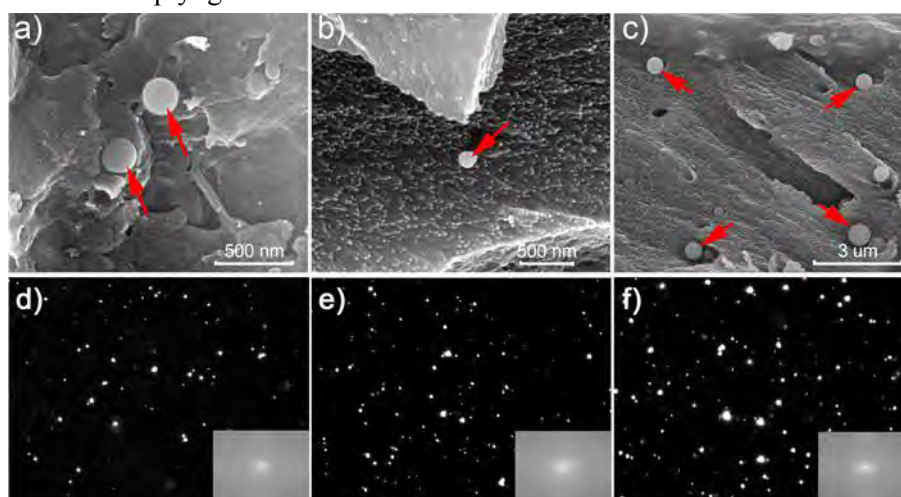


Figure 10. Cross-section SEM images of cPI films doped with a) Al_2O_3 200 nm 3.0 wt%, b) SiO_2 200-300 nm 3.0 wt%, and c) SiO_2 400-600 nm 3.0 wt%. The arrows denote nanoparticles. Optical microscopic images ($125 \times 93.75 \mu\text{m}^2$) cPI films doped with of d) Al_2O_3 200 nm 3.0 wt%, e) SiO_2 200-300 nm 3.0 wt%, and f) SiO_2 400-600 nm 3.0 wt%.

We attribute them to the following possible reasons: (a) the gel in solutions, which could not be eliminated by filtration, turned into gel particles after annealing; (b) a small part of nanoparticles were not completely dispersed; and (c) those particles (gel particles and agglomerated nanoparticles) embedded at different depths in the films were easily out of focus due to the limited depth of field of

the microscope, which further expanded the spots they exhibited.

3.2.3. Influence of Refractive Index

The atomic force microscope (AFM) images (Figure 11) exhibit the morphology of the doped cPI films. Almost the height of all bumps were less than 70 nm, and their smooth surfaces (RMS less than 8 nm)precluded the possibility that the high haze of the doped film resulted from surface roughness.

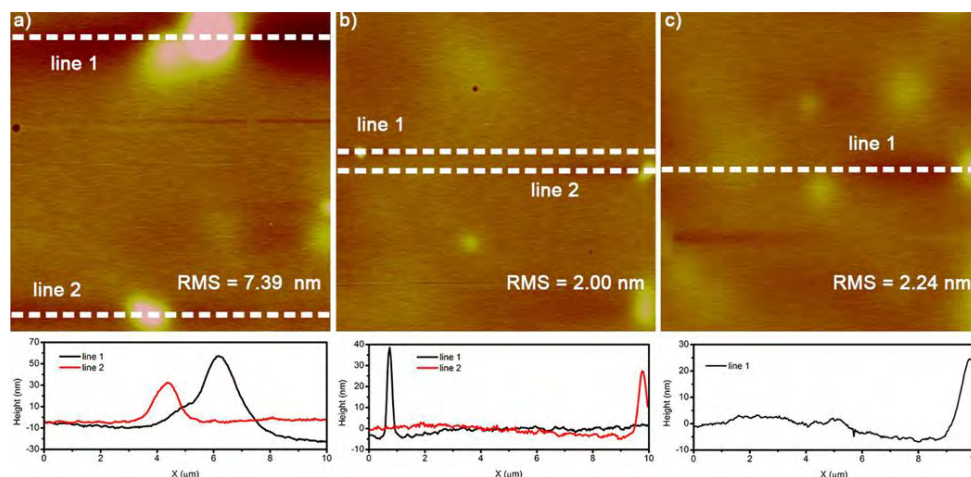


Figure 11. AFM images ($10 \times 10 \mu\text{m}^2$) of cPI-1 films doped with a) Al_2O_3 200 nm 3.0 wt%, b) SiO_2 200-300 nm 3.0 wt%, and c) SiO_2 400-600 nm 3.0 wt%.

Compared with the pure cPI-1 film (Figure 12a), there was no obvious decrease of transmittance when doped with SiO_2 200-300 nm 3.0wt%. But a significant reduction was observed when doped with Al_2O_3 200 nm 3.0wt%. In the case of cPI-2(Figure 12b), both of the above two nanoparticles led to a significant reduction to transmittance and the decrease was more obvious for the film doped with SiO_2 200-300nm 3.0 wt%. For the haze of the doped cPI films, notable improvements of haze for cPI-1 and cPI-2 were obtained due to the doping of nanoparticles. Although haze of the cPI-1 film doped with SiO_2 200-300 nm 3.0wt% was remarkably higher than the one ofthe pure film, but it is about half lower than that of the film doped with Al_2O_3 200 nm 3.0wt%. The case for cPI-2 was opposite to cPI-1.

For the particle scattering, the dimensionless size parameter x and refractive index ratio of particle to the medium m , which are defined as below (eq 2 and eq3). On the basis of the value of x , models of light scattering can be roughly divided into three domains: Rayleigh scattering (small particle compared to wavelength of light, $x < 1$), Mie scattering (particle about the same size as wavelength of light, $x \approx 1$, valid only for spheres),and geometric scattering (particle much larger than wavelength of light, $x > 1$).

$$x = \frac{\pi D}{\lambda} \quad (2)$$

$$m = \frac{n_{\text{par}}}{n_{\text{amb}}} \quad (3)$$

In the above equation, the D , λ , n_{par} , and n_{amb} are the diameter of a particle sphere, wavelength of incident light, refractive index of the particle sphere, and refractive index of the ambient medium, respectively. In this paper, Al_2O_3 spheres with average diameters of 200 nm ($x_1 = 1.1424$, computed with $\lambda = 550$ nm) as well as SiO_2 spheres with diameter of 200-300 nm ($1.1424 = x_1 < x < x_2 = 1.7136$) and 400-600 nm ($2.2848 = x_3 < x < x_4 = 3.4274$) were doped in two kinds of cPI films at different concentrations, respectively. The Mie theory can be reasonably applied to this paper according to the

values of x . Transmittance and haze of these doped cPI films were measured to study their relationship with differences of refractive indices between polyimide materials and nanoparticles, particle sizes, and doping concentrations. Haze of the films in this paper was calculated by the following formula (eq 4):

$$\text{haze} = \frac{T_{\text{int}} - T_{\text{nor}}}{T_{\text{int}}} \times 100\% \quad (4)$$

where T_{nor} denote the transmittance measured in normal direction, and T_{int} denote the transmittance measured with anintegrating sphere. Without special description, transmittance in this paper refers to T_{int} .

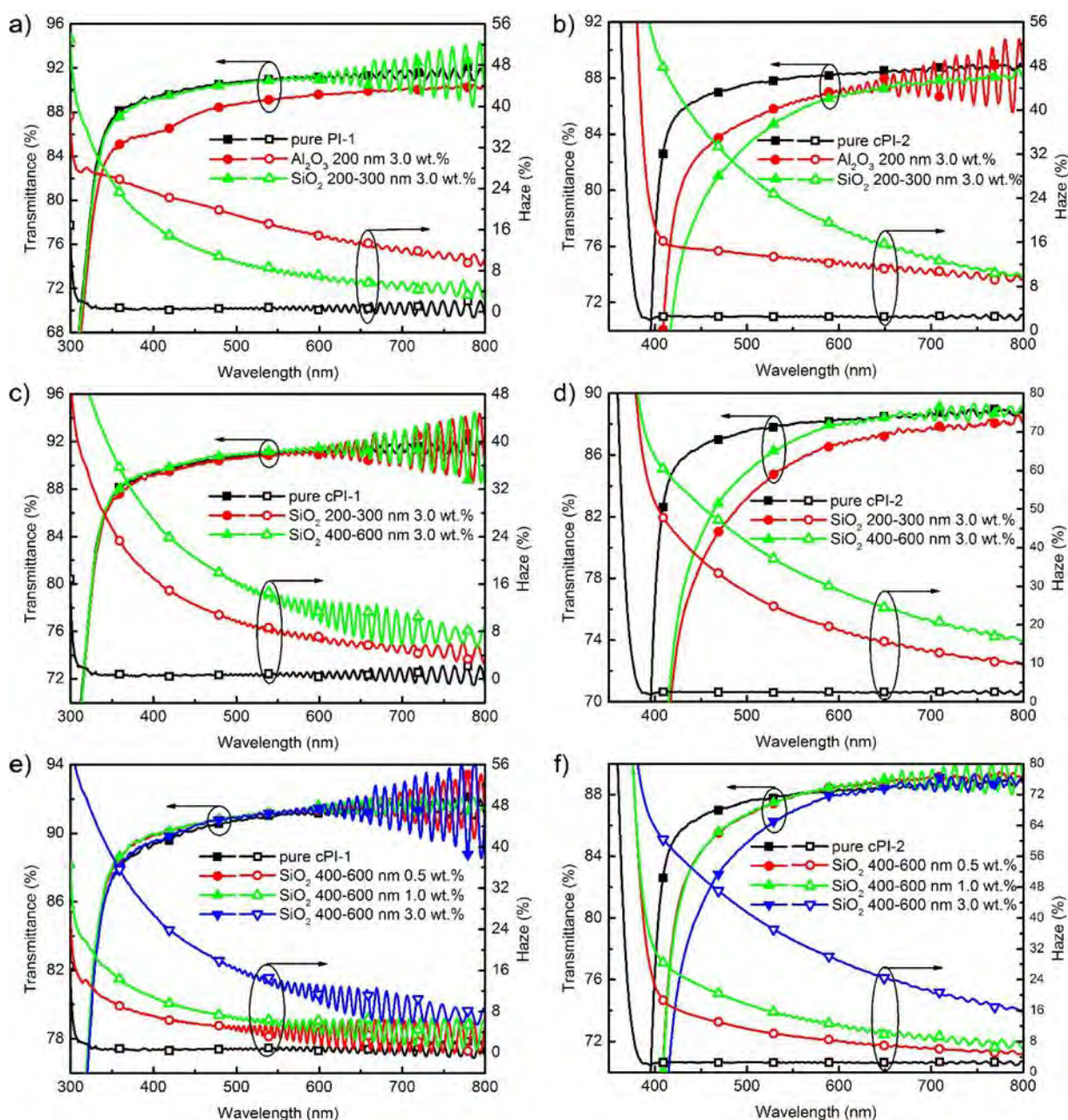


Figure 12. Transmittance and haze of polyimide films made from cPI-1 and cPI-2. a) cPI-1, b) cPI-2 doped with Al_2O_3 200 nm 3.0 wt% or SiO_2 200-300nm 3.0 wt%. c) cPI-1, d) cPI-2 doped with SiO_2 200-300 nm 3.0 wt% or SiO_2 400-600 nm 3.0 wt%. e) cPI-1, f) cPI-2 doped with SiO_2 400-600 nm at concentration of 0.5 wt%, 1.0 wt%,

and 3.0 wt%, respectively. The thickness of the films is 12.5 μm. Solid marks represent transmittance and open marks represent haze.

Let m_1 , m_2 , m_3 , and m_4 be the refractive indices of SiO₂ and Al₂O₃ relative to the ambient medium cPI-1 and cPI-2 at wavelength of 550 nm. According to Figure 2 and eq 2, we have

$$m_1 = \frac{n_{\text{SiO}_2}}{n_{\text{cPI-1}}} = 0.9416, \quad m_2 = \frac{n_{\text{SiO}_2}}{n_{\text{cPI-2}}} = 0.8752, \quad m_3 = \frac{n_{\text{Al}_2\text{O}_3}}{n_{\text{cPI-1}}} = 1.1413, \quad m_4 = \frac{n_{\text{Al}_2\text{O}_3}}{n_{\text{cPI-2}}} = 1.0608,$$

$m_1 < m_2 < m_4 < m_3$. On the basis of these m values, the scattering efficiencies (Q_{sca}) and backward scattering efficiencies (Q_{b}) versus size parameter x calculated by Mie theory were shown in Figure 13. $\forall x \in [x_2, x_3]$, we have $Q_{\text{sca-SiO}_2} < Q_{\text{sca-Al}_2\text{O}_3}$ and $Q_{\text{b-SiO}_2} < Q_{\text{b-Al}_2\text{O}_3}$ (Figure 13a), which refers to stronger total and backward scattering effects for Al₂O₃ with constant incident light that results in a larger reduction of transmittance and increase of haze with respect to the pure cPI-1 film, respectively. The similar explanation also works for cPI-2 (Figures 12b and 13b) doped with SiO₂ 200-300nm 3.0wt% and Al₂O₃ 200 nm 3.0wt%, respectively. On the whole, larger refractive index differences between materials of the films and nanoparticles contributes to higher haze of the film and larger reduction of transmittance.

3.3.4. Influence of Particle Size

Figure 12c,d shows the transmittance and haze of films doped with different sizes of SiO₂ particles at 3.0wt%. For the case of cPI-1, both performances in transmittance were substantially the same, except the slight difference that the film doped with particles in larger size showed higher transmittance, which was almost negligible. This phenomenon also appeared in the doped cPI-2 films, but a little bit more remarkable. Both cPI-1 and cPI-2 films doped with different sizes of SiO₂ nanoparticles at 3.0wt% showed a significantly improved haze, and the haze of the films doped with larger size of particles was roughly two times higher than those doped with the smaller ones.

Along the black lines with solid rectangle marks in Figure 13, $\forall x \in [x_1, x_4]$ makes $Q_{\text{sca}}(x)$ a monotonic increasing function, that is, a larger particle size contributes a larger $Q_{\text{sca}}(x)$ which leads to a large haze of the doped film. This is what makes the haze of cPI films doped with SiO₂ 400-600 nm 3.0wt% higher than those doped with SiO₂ 200-300nm 3.0wt%.

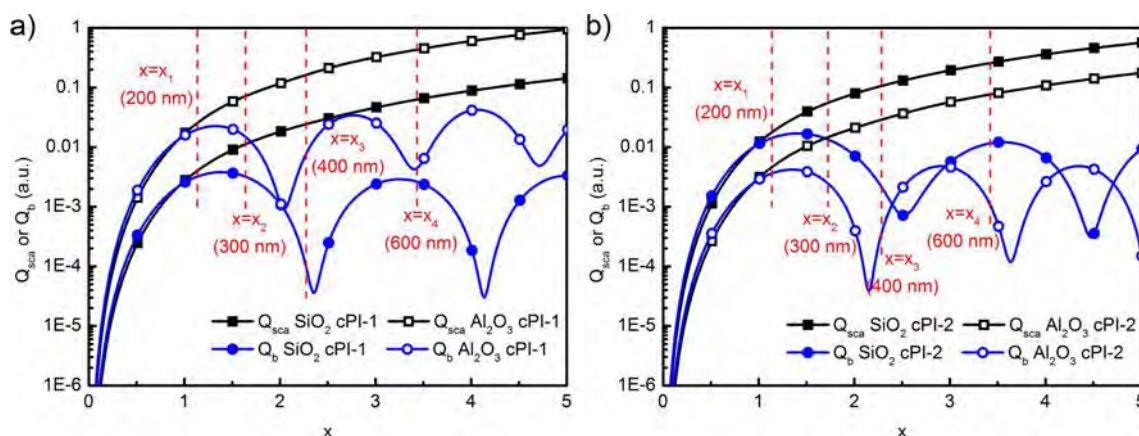


Figure 13. Scattering efficiencies and backward scattering efficiencies calculated by Mie theory for spherical SiO₂ and Al₂O₃ nanoparticles doped in a) cPI-1 and b) cPI-2.

Furthermore, as shown in Figure 13, the influence of particle size on backward scattering is periodic. Although the corresponding values of x to particle sizes belong to different periods, almost $\forall x \in [x_1, x_2]$ makes $Q_{\text{b}}(x)$ larger than that of $\forall x \in [x_3, x_4]$ (blue lines with solid circle marks in Figure 12). As a consequence, cPI films doped with SiO₂ 200-300nm 3.0 wt% suffer stronger

backward scattering than those doped with SiO₂ 400-600 nm 3.0wt%. Thus, the cPI films doped with SiO₂ 200-300nm 3.0wt% show lower transmittance than those doped with SiO₂ 400-600 nm 3.0wt%.

3.3.5. Influence of Doping Concentration

Figure 11e, f show the transmittance and haze of the cPI films doped with SiO₂ 400-600 nm at different concentration. The number of the particles per unit volume was increased with higher doping concentration, which brought about larger Q_{sca} and Q_b , therefore, the transmittance and haze of these cPI films were affected to a different extent. Specifically, the haze of all these cPI films was rapidly improved due to a higher Q_{sca} . Meanwhile, transmittance of the cPI films showed successively increased reductions with the increasing of doping concentration due to a higher Q_b , among which the cPI-2 films doped at concentration of 3.0wt% showed a more significant reduction of transmittance than those doped at lower concentrations.

Namely, transmittance and haze of films made from different cPI have different sensitivities on doping concentration. In practice, a balance between transmittance and haze can be found by controlling the doping concentration depending on the specific needs.

4. CONCLUSIONS

In conclusion, we have successfully synthesized a series of isomeric PI films. All of the films shown outstanding thermal resistant attributing to disturbed chain stacking by a twist/nonplanar steric structure of the DAPI based diamine fragments. Systematic study revealed that PI based on 5-DAPI displayed much better optical and mechanical properties than 6-DAPI. And a polymorphic dianhydride 8FDA and a transparent polyimide based on 8FDA were reported. Compared with the widely used dianhydride 6FDA and HPMDA, 8FDA-based transparent PI films showed much better thermal and dimensional stabilities.

Transparent colorless PI films doped/undoped with different sizes of nanoparticles were prepared. A systematic study on the transmittance spectra and haze of these films was conducted. It was found that the transmittance varies with the film thickness and the wavelength of the incident light.

There is a minimum film thickness to avoid the oscillation of transmittance spectra. For cPI films, the thickness should be larger than 12.5 μm . For the potential application in large-area flexible OLED lighting panels, cPI substrates with high haze and acceptable transmittance are favorable, and nanoparticle doping is apparently a cost-effective method. The transmittance and haze of the film can be intuitively regulated by simply doping of nanoparticles, which is a result from the joint effects of the refractive index differences of the materials, particle size, and doping concentration. With the approaching of the refractive indices of nanoparticles and cPI films (the relative refractive index m approaches 1), the reduction of transmittance and haze of the doped films decreases simultaneously, which can be compensated by the increase of size parameter (x) and doping concentration.

Acknowledgements

The authors thank the National Natural Science Foundation of China (Grant No. 21574049) and the National High Technology Research and Development Program of China (863 Program, No. 2015AA033404) for financial support.

References

- [1] I.V. Farr, T.E. Glass, Q. Ji, J.E. McGrath, Synthesis and characterization of dia-minophenylindane based polyimides via ester-acid solution imidization, High Perform. Polym. 9 (1997) 345-352.
- [2] F. Li, W.J. Wan, J.C. Lai, F. Liu, H.X. Qi, X.S. Li, X.Z. You, Investigations on the polyimides derived from unfunctionalized symmetric cyclopentyl-containing alicyclic cardo-type dianhydride, J. Appl. Polym. Sci. 132 (2015), 42670(1-10).

- [3] W. Chen, W. Chen, B. Zhang, S. Yang, C.-Y. Liu, Thermal imidization process of polyimide film: interplay between solvent evaporation and imidization, *Polymer* 109 (2017) 205-215.
- [4] Y. Zhuang, J.G. Seong, Y.S. Do, H.J. Jo, M.J. Lee, G. Wang, M.D. Guiver, Y.M. Lee, Effect of isomerism on molecular packing and gas transport properties of poly(benzoxazole-co-imide), *Macromolecules* 47 (2014) 7947-7957.
- [5] Z. Hu, M. Wang, S. Li, X. Liu, J. Wu, Ortho alkyl substituents effect on solubility and thermal properties of fluorenyl cardo polyimides, *Polymer* 46 (2005)5278-5283.
- [6] M.X. Ding, Isomeric polyimides, *Prog. Polym. Sci.* 32 (2007) 623-668.
- [7] Wu, S.; Hayakawa, T.; Kikuchi, R.; Grunzinger, S.J.; Kakimoto, M. Synthesis and characterization of semiaromatic polyimides containing poss in main chain derived from double-decker-shaped silsesquioxane. *Macromoleclars* 2007, 40, 5698-5705.
- [8] Hu, X.; Yan, J.; Wang, Y.; Mu, H.; Wang, Z.; Cheng, H.; Zhao, F.; Wang, Z. Colorless polyimides derived from 2R,5R,7S,10S-naphthanetetracarboxylic dianhydride. *Polym. Chem. UK* 2017, 8, 6165–6172.
- [9] Hu X., Yan J., Wang Y., et al. Colorless polyimides derived from 2R, 5R, 7S, 10S-naphthanetetracarboxylic dianhydride. *Polymer Chemistry*, 2017, 8(39): 6165-6172
- [10] Yu X., Liang W., Cao J., et al. Mixed rigid and flexible component design for high-performance polyimide films. *Polymers*, 2017, 9(9): 451
- [11] Nolan, D.; Senaratne, W.; Baker, D.; Liu, L. Optical Scattering from Nanostructured Glass Surfaces. *Int. J. Appl. Glass Sci.* 2015, 6,345-355.
- [12] Biswas, S.; Kar, G. P.; Bose, S. Tailor-Made Distribution of Nanoparticles in Blend Structure toward Outstanding Electromagnetic Interference Shielding. *ACS Appl. Mater. Interfaces* 2015, 7, 25448-25463.